Comparative Kinetics of Cofactor Association and Dissociation for the Human and Trypanosomal *S*-Adenosylhomocysteine Hydrolases. 1. Basic Features of the Association and Dissociation Processes†

Qing-Shan Li,‡ Sumin Cai,§ Ronald T. Borchardt,‡ Jianwen Fang,|| Krzysztof Kuczera,§,⊥ C. Russell Middaugh,‡ and Richard L. Schowen*,‡,§,⊥

Departments of Pharmaceutical Chemistry, Chemistry, and Molecular Biosciences and Bioinformatics Core Facility, The University of Kansas, Lawrence, Kansas 66047

Received January 26, 2007

ABSTRACT: The *S*-adenosyl-L-homocysteine (AdoHcy) hydrolases catalyze the reversible conversion of AdoHcy to adenosine and homocysteine, making use of a catalytic cycle in which a tightly bound NAD^+ oxidizes the 3′-hydroxyl group of the substrate at the beginning of the cycle, activating the 4′-CH bond for elimination of homocysteine, followed by Michael addition of water to the resulting intermediate and a final reduction by the tightly bound NADH to give adenosine. The equilibrium and kinetic properties of the association and dissociation of the cofactor NAD^+ from the enzymes of *Homo sapiens* (Hs-SAHH) and *Trypanosoma cruzi* (Tc-SAHH) are qualitatively similar but quantitatively distinct. Both enzymes bind NAD^+ in a complex scheme. The four active sites of the homotetrameric apoenzyme appear to divide into two numerically equal classes of active sites. One class of sites binds cofactor weakly and generates full activity very rapidly (in less than 1 min). The other class binds cofactor more strongly but generates activity only slowly (>30 min). In the case of Tc-SAHH, the final affinity for NAD^+ is roughly micromolar and this affinity persists as the equilibrium affinity. In the case of Hs-SAHH, the slow-binding phase terminates in micromolar affinity also, but over a period of hours, the dissociation rate constant decreases until the final equilibrium affinity is in the nanomolar range. The slow binding of NAD^+ by both enzymes exhibits saturation kinetics with respect to the cofactor concentration; however, binding to Hs-SAHH has a maximum rate constant around 0.06 s^{-1}, while the rate constant for binding to Tc-SAHH levels out at 0.006 s^{-1}. In contrast to the complex kinetics of association, both enzymes undergo dissociation of NAD^+ from all four sites in a single first-order reaction. The equilibrium affinities of both Hs-SAHH and Tc-SAHH for NADH are in the nanomolar range. The dissociation rate constants and the slow-binding association rate constants for NAD^+ show a complex temperature dependence with both enzymes; however, the cofactor always dissociates more rapidly from Tc-SAHH than from Hs-SAHH, the ratio being around 80-fold at 37 °C, and the cofactor binds more rapidly to Hs-SAHH than to Tc-SAHH above ∼16 °C. These features present an opening for selective inhibition of Tc-SAHH over Hs-SAHH, demonstrated with the thioamide analogues of NAD^+ and NADH. Both analogues bind to Hs-SAHH with ∼40 nM affinities but much more weakly to Tc-SAHH (0.6−15 μM). Nevertheless, both analogues inactivated Tc-SAHH 60% (NAD^+ analogue) or 100% (NADH analogue) within 30 min, while the degree of inhibition of Hs-SAHH approached 30% only after 12 h. The rate of loss of activity is equal to the rate of dissociation of the cofactor and thus 80-fold faster at 37 °C for Tc-SAHH.

SAHH[1] (*1*) catalyzes the reversible interconversion of AdoHcy to adenosine (Ado) and homocysteine (Hcy), with physiological conditions favoring the hydrolytic reaction. SAHH is the only known catabolic enzyme of AdoHcy, a powerful transmethylation inhibitor, and thus an endogenous regulator of methylation reactions (*1*) and a key enzyme of the methyl cycle. Inhibition of the expression of SAHH in mammalian cells causes an increase in the cellular level of AdoHcy and inhibition of AdoMet-dependent methyltransferases, thereby affecting the methylation status of nucleic

† This study was supported by Grant GM-29332 from the National Institute of General Medical Sciences and by the K-INBRE Bioinformatics Core, NIH Grant P20 RR016475.

* To whom correspondence should be addressed: Department of Pharmaceutical Chemistry, 2095 Constant Ave., The University of Kansas, Lawrence, KS 66047. Phone: (785) 864-4080. Fax: (785) 864-5736. E-mail: rschowen@ku.edu.

‡ Department of Pharmaceutical Chemistry.

§ Department of Molecular Biosciences.

|| Bioinformatics Core Facility.

⊥ Department of Chemistry.

[1] Abbreviations: 2×YT, 2× yeast extract tryptone; Ado, adenosine; AdoHcy, *S*-adenosyl-L-homocysteine; CD, circular dichroism; DSC, differential scanning calorimetry; EDTA, ethylenediaminetetraacetic acid; FPLC, fast protein liquid chromatography; Hcy, L-homocysteine; HPLC, high-performance liquid chromatography; Hs-SAHH, SAHH from *Homo sapiens* (human placenta); NAD^+, β-nicotinamide adenine dinucleotide; NADH, β-nicotinamide adenine dinucleotide, reduced form; SAHH, *S*-adenosyl-L-homocysteine hydrolase (EC 3.1.1.1); S-NAD^+, β-thionicotinamide adenine dinucleotide; S-NADH, β-thionicotinamide adenine dinucleotide, reduced form; Tc-SAHH, SAHH from *Trypanosoma cruzi*.

10.1021/bi700170m CCC: $37.00
Published on Web 04/21/2007

acids, proteins, phospholipids, and small molecules (*2*). Parasites such as *Trypanosoma cruzi*, *Leishmania donovani*, and *Plasmodium falciparum* express their own AdoHcy hydrolases (*3*−*5*). Inhibition of parasitic SAHH suppresses the growth of these parasites. For example, 3-deazaaristeromycin and 2′,3′-dihydroxycyclopentanyladenine inhibit the growth of *L. donovani* (*6*). Neplanocin A and 4′,5′-didehydro-5′-fluoroadenosine inhibit the growth of *P. falciparum* (*7*, *8*), and 7-deaza-5′-noraristeromycin and 3′-deoxyadenosine have inhibitory effects on the growth of *Trypanosoma* species (*9*, *10*). Such observations suggest the possible utility of SAHH inhibitors as antiparasitic agents if inhibitors specific for the parasite enzymes can be found.

SAHHs are highly conserved homotetrameric proteins (*11*−*13*). Hs-SAHH has 432 amino acids per subunit, and its amino acid sequence is ∼70% identical with those of the enzymes from *T. cruzi*, *L. donovani*, and *P. falciparum* (*1*, *3*). The enzymes from human and rat sources (the latter being 97% identical to the human enzyme) have been well studied, and X-ray crystallographic structures of various complexes of the human placenta and rat liver enzymes are available (*14*, *15*). Recently, the structure of SAHH from *P. falciparum* was published (*13*), and the structure of Tc-SAHH with bound Neplanocin A (unpublished data of Q.-S. Li and W. Huang) has been determined. Comparisons of the sequence and structure of Hs-SAHH with those of Tc-SAHH and the *P. falciparum* enzyme show a strong similarity among the three enzymes.

However, it was reported that the enzymes from *T. cruzi* and *L. donovani* bound NAD^+ less tightly than the human enzyme (*3*, *4*), and we also observed that the enzyme from *P. falciparum* bound NAD^+ less tightly than the human enzyme (unpublished data). Therefore, the cofactor-binding site and its properties have become a focus of interest for finding those distinguishing features among these enzymes that might permit differential inhibition. In this work, we have systematically analyzed the comparative kinetics of cofactor association and dissociation and their temperature dependences for Hs-SAHH and Tc-SAHH.

MATERIALS AND METHODS

Expression and Purification of Hs-SAHH and Tc-SAHH. The expression of the two enzymes was basically the same as that previously described (*3*, *4*). Briefly, in separate experiments, the gene encoding each enzyme was inserted into the pPROK-1 vector (Clontech), and the recombinant plasmids were transferred into *Escherichia coli* strain JM109. The transformed *E. coli* cells grew in 1 L of 2×YT medium containing ampicillin (100 mg/L) at 37 °C. When the absorbance at 600 nm reached 0.4−0.8, 1 mM isopropyl 1-thio-β-D-galactopyranoside was added to induce protein expression during the incubation at 37 °C for 8 h for Hs-SAHH and at 25 °C for 12 h for Tc-SAHH.

The procedures for purification of the two enzymes were the same except that 50 μM NAD^+ was added to the buffer before purification of Tc-SAHH. The harvested *E. coli* cells containing the enzyme were stored at −80 °C. Preparation of a cell-free extract was carried out as previously described (*3*, *4*). The enzyme was purified from the cell-free extract by means of four columns in a FPLC system (Amersham Biosciences). The buffer during all purification processes was 50 mM Tris-HCl (pH 7.4) containing 1 mM EDTA. A typical procedure is as follows. The cell-free extract was loaded onto a Q-Sepharose Fast Flow column (26/10), and the enzyme was eluted with 50−150 mM NaCl in buffer. The enzyme sample was then passed through a Hiload Phenyl-Sepharose column (26/10) and a Hiload Superdex 200 column (16/60) and placed on a MonoQ column (10/10) from which the purified enzyme was eluted with 50−300 mM NaCl in buffer.

Enzyme Activity Assay and Determination of Kinetic Properties. SAHH activity was assayed in the synthetic direction by measuring the rate of formation of AdoHcy from Ado and Hcy by use of HPLC as previously described (*16*, *17*). The enzyme activity in the hydrolytic direction was determined by coupling the conversion of AdoHcy to Ado and Hcy to the deamidation of Ado with catalysis by Ado deaminase (*17*).

Determination of Apoenzyme Concentrations by Titration with NAD^+. The apoenzyme was prepared as previously described (*18*). All enzyme and apoenzyme concentrations used in this paper are given as formal concentrations of the monomeric subunit. Because NAD^+ binds to both Hs-SAHH and Tc-SAHH very tightly at 22 °C (K_d below 50 nM at 22 °C for both enzymes), the concentration of the apoenzyme can be determined by NAD^+ titration. To a volume of 10 μL containing initially 40 μM apoenzyme were added successive 10 μL portions of a NAD^+ stock solution to produce concentrations from 1.5 to 180 μM. The solutions were then incubated at 22 °C until no further increase was observed in enzyme activity (usually from 20 to 90 min). Enzyme activity was measured in the hydrolytic direction. Concentrations of NAD^+ were increased to approximately 9 times the saturation value, and the enzyme concentration (monomers) was thought to be equal to the concentration of enzyme-bound NAD^+ under saturation conditions. At NAD^+ concentrations below the equivalence point, the activity is equal to $\gamma[NAD^+]$, where γ is the activity per occupied active site and is equal to the slope of the plot of activity versus $[NAD^+]$. Above the equivalence point, the slope becomes zero and the intercept becomes $\gamma[E]_{tot} = \gamma[NAD^+]_{bound}$, where $[E]_{tot}$ is the total enzyme concentration expressed as monomers. The intercept/slope ratio thus yields the relationship $[E]_{tot} = [NAD^+]_{bound}$. The values of $[E]_{tot}$ corresponded closely to the values calculated from the protein concentration.

Determination of Rate Constants for Association of NAD^+ and NADH with Apoenzyme (apparent first-order rate constant k_{app} and apparent second-order rate constant k_{on}). Typically, to a 50 μL solution [50 mM phosphate buffer (pH 7.4) and 1 mM EDTA] containing 2 μM apoenzyme were added successive portions of 50 μL of a stock solution to produce concentrations of NAD^+ from 1 to 300 μM. Samples were taken for activity assay at measured times during incubation at the desired temperature. The measured activities (A) were either converted to the amount of enzyme−NAD^+ complex or used directly in eq 1.

$$A = A_f - (A_f - A_o)[\exp(-k_{app}t)] \quad (1)$$

where A is the activity measured at time t, A_o is the activity at the apparent time zero (reflecting reaction during the dead time of the experiment), A_f is the activity at the end of the experiment, and k_{app} is a first-order rate constant for

association that generally will be a function of [NAD^+]. At 5 μM NAD^+, A_o is quite small and k_{app} is approximately proportional to [NAD^+]; an apparent second-order rate constant for the association reaction (k_{on}) was therefore calculated from data at this concentration as $k_{on} = k_{app}/[NAD^+]$ and was used in the calculation of the equilibrium dissociation constant (see below).

In the measurement of k_{app} for NADH, the bound NADH was monitored by a fluorescence method as previously described (*16*).

Determination of the Rate Constants for Dissociation of NAD^+ from Hs-SAHH and Tc-SAHH (k_{off}). A 200 μL solution containing 4 μM SAHH, 80 units/mL alcohol dehydrogenase, 30 mM 2-propanol, 2 mM NADH, and 1 mM EDTA in a 50 mM phosphate buffer at pH 7.4 was incubated at a desired temperature. Samples were taken at measured times for the determination of enzyme activity. The concentration of NADH, binding of which to the enzyme rendered the dissociation of NAD^+ irreversible, was in large excess over the enzyme concentration and did not significantly change during the experiments. As a control for thermal inactivation of the enzyme, the activity of SAHH was also determined under the same conditions described above except that no NADH or alcohol dehydrogenase was present. The time dependence of the relative enzyme activity (A/A_o) in both the dissociation experiment and the thermal inactivation control fitted to eq 2, which is equivalent to eq 1 when $A_f = 0$.

$$A/A_o = \exp(-k_{obs}t) \quad (2)$$

In the control experiment for loss of activity by thermal inactivation, $k_{obs} = k_{ina}$, the first-order rate constant for thermal inactivation of the enzyme. When thermal inactivation and NAD^+ dissociation were occurring simultaneously, $k_{obs} = k_{tot} = k_{ina} + k_{off}$, where k_{off} is the apparent first-order rate constant for dissociation of NAD^+. The rate constant k_{off} for NAD^+ dissociation was then obtained from the equation $k_{off} = k_{tot} - k_{ina}$.

Determination of Thermal Stability by Circular Dichroism (CD) Spectroscopy. CD spectra were measured with a Jasco J-720 spectropolarimeter equipped with a Peltier temperature controller. Enzyme samples [0.1 mg/mL in 50 mM phosphate buffer (pH 7.4) and 1 mM EDTA] were contained in 0.1 cm path length cells. A resolution of 0.2 nm and a scanning speed of 20 nm/min with a 2 s response time were employed. Spectra presented are an average of three consecutive spectra. For the thermal stability experiment, the signal at 222 nm was measured at 0.1 °C intervals with use of a temperature ramp rate of 60 °C/h.

Thermal Stability Measurements by Differential Scanning Calorimetry (DSC). Apoenzyme samples (2 mg/mL) were degassed under mild vacuum for 15 min before thermograms were obtained with a Microcal (Northampton, MA) DSC instrument. A 0.9 mL solution of buffer containing 50 mM phosphate and 1 mM EDTA (pH 7.4) was placed in the reference cell, and the apoenzyme sample in the same buffer was placed in the sample cell. Thermograms from 25 to 80 °C were collected at a scan rate of 60 °C/h. Similar scans obtained with buffer in both the reference and sample cells were subtracted from the apoenzyme thermograms.

Determination of the Equilibrium Dissociation Constants (K_d) for NAD^+ and NADH. The equilibrium dissociation constants for NAD^+ were calculated from the ratio of the dissociation and association rate constants ($K_d^{NAD^+} = k_{off}/k_{on}$) which were measured as described above.

The equilibrium dissociation constants for NADH were calculated from the loss of enzyme activity as NADH replaces NAD^+ in the enzyme active sites. In the absence of added NADH, the activity of the enzyme will be proportional to the fraction of enzyme associated with NAD^+ as in eq 3

$$A([NADH]=0) = \alpha E_{tot}[[NAD^+]/(K_d^{NAD^+} + [NAD^+])] \quad (3)$$

where α is a known function of the enzyme kinetics [for the hydrolytic direction of SAHH action, α is proportional to $k_{cat}[AdoHcy]/(K_M + [AdoHcy])$ and E_{tot} is the total concentration of enzyme in all forms (E and E−NAD^+)]. In the presence of NADH, the activity A is proportional to a total enzyme concentration given by eq 4a

$$E_{tot} = [E] + [E-NAD^+] + [E-NADH] = [E-NAD^+](K_d^{NAD^+}/[NAD^+] + 1 + K_d^{NAD^+}[NADH]/K_d^{NADH}[NAD^+]) \quad (4a)$$

so that the activity is given by eq 4b.

$$A = \alpha E_{tot}/(K_d^{NAD^+}/[NAD^+] + 1 + K_d^{NAD^+}[NADH]/K_d^{NADH}[NAD^+]) \quad (4b)$$

Combining eqs 3 and 4b then gives eq 5:

$$A([NADH]=0)/A = 1 + ([NADH]/K_d^{NADH})(K_d^{NAD^+}/(K_d^{NAD^+} + [NAD^+])) \quad (5)$$

Because $K_d^{NAD^+}$ is known, nonlinear least-squares fitting (Origin, Microcal) of A as a function of [NADH] to eq 5 then yields K_d^{NADH}.

Inhibition of Hs-SAHH and Tc-SAHH by the NAD(H) Analogues, S-NAD^+ and S-NADH. Thionicotinamide adenine dinucleotide (S-NAD^+) was obtained from Sigma (T7375). The reduced form of thionicotinamide adenine dinucleotide (S-NADH) was prepared from the oxidized form by use of alcohol dehydrogenase (Sigma, A-3263). Reduction of the oxidized form of S-NAD^+ was followed by HPLC using the procedure described for the enzyme activity assay. The loss of activity of Hs-SAHH and Tc-SAHH was monitored as described above, and equilibrium dissociation constants of the thione analogues S-NAD^+ and S-NADH were calculated by the same method used for NADH. To determine k_{off} for S-NAD^+ and S-NADH, 20 μL volumes of solutions of Hs-SAHH or Tc-SAHH reconstituted with S-NAD^+ and S-NADH (and thus catalytically inactive) were incubated in the presence of 5 mM NAD^+ at 37 °C. Samples were taken at the desired times, and the activity was measured. The fractional gain in activity with time was taken to be equal to the fractional release of S-NAD^+ or S-NADH.

RESULTS

Kinetics of the Dissociation of NAD^+ from Hs-SAHH and Tc-SAHH. Figure 1 shows the loss of fractional activity as

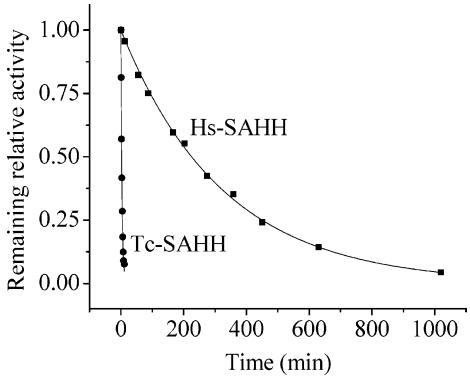

FIGURE 1: Time course of the loss of enzyme activity at 37 °C as NAD^+ dissociates from Hs-SAHH [shallow curve; $k_{obs} = k_{off} = (5.1 \pm 0.1) \times 10^{-5}$ s^{-1}] and Tc-SAHH [steep curve; $k_{obs} = k_{off} = (4.7 \pm 0.1) \times 10^{-3}$ s^{-1}]. The solid lines are exponential functions (eq 2).

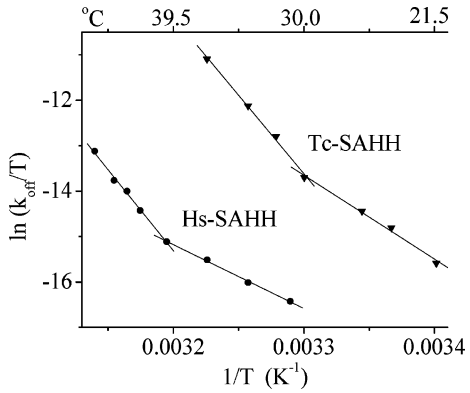

FIGURE 2: Temperature dependence of the rate constant for dissociation of NAD^+ from Hs-SAHH (bottom curve) and from Tc-SAHH (top curve). The lines are intersecting Eyring plots with the parameters given in Table 1.

a function of time as NAD^+ dissociates from Hs-SAHH and Tc-SAHH. The data are described by a simple single-exponential function (eq 2) and after correction for thermal inactivation (negligible under these circumstances) yield the dissociation constant k_{off}.

Temperature Dependence of the Kinetics of the Dissociation of NAD$^+$ from Tc-SAHH and Hs-SAHH. Figure 2 presents Eyring plots of the first-order rate constants k_{off} for dissociation of the cofactor NAD^+ from Hs-SAHH (from 31 to 45.5 °C) and from Tc-SAHH (from 21 to 37 °C). The Eyring plots are nonlinear for both enzymes, consisting of a linear low-temperature regime and a linear high-temperature regime. Two expressions (eqs 6a and 6b) were considered for fitting of the data, corresponding to mechanistic models in the Discussion.

$$k_{off}/(kT/h) = \exp(\Delta S^{\ddagger}_{/}/R - \Delta H^{\ddagger}_{/}/RT) + \exp(\Delta S^{\ddagger}_{h}/R - \Delta H^{\ddagger}_{h}/RT) \quad (6a)$$

$$k_{off}/(kT/h) = [\exp(\Delta S^{\ddagger}_{/}/R - \Delta H^{\ddagger}_{/}/RT)](1/\{1 + [\exp(\Delta S^{\circ}_{/h}/R) - \Delta H^{\circ}_{/h}/RT]\}) + [\exp(\Delta S^{\ddagger}_{h}/R - \Delta H^{\ddagger}_{h}/RT)]([\exp(\Delta S^{\circ}_{/h}/R) - \Delta H^{\circ}_{/h}/RT]/\{1 + [\exp(\Delta S^{\circ}_{/h}/R - \Delta H^{\circ}_{/h}/RT)]\}) \quad (6b)$$

The expression of eq 6a, where the subscript / denotes the quasi-thermodynamic parameters of activation for the low-temperature regime and the subscript h denotes those for the high-temperature regime, corresponds to parallel dissociation reactions with different activation parameters. Attempts to fit this expression to the data produced very large errors in the adjustable parameters and plots that failed to intersect some of the points. This expression produces curvature that is too gentle to correspond to all the data.

The expression of eq 6b allows for a more abrupt shift from the low-temperature to the high-temperature regime in a transition with equilibrium thermodynamic parameters $\Delta S^{\circ}_{/h}$ and $\Delta H^{\circ}_{/h}$. This approach requires determination of six adjustable parameters. Since the data sets contain only seven (Tc-SAHH) and eight (Hs-SAHH) experimental points, the full-scale fitting exercise is futile. Therefore, the two temperature regimes were independently fitted to an Eyring expression (eqs 6c and 6d) for each set of data.

$$k_{off}/(kT/h) = \exp(\Delta S^{\ddagger}_{/}/R - \Delta H^{\ddagger}_{/}/RT) \quad (6c)$$

$$k_{off}/(kT/h) = \exp(\Delta S^{\ddagger}_{h}/R - \Delta H^{\ddagger}_{h}/RT) \quad (6d)$$

The values of the quasi-thermodynamic parameters of activation are given in Table 1. The conversion temperature T_o for passage from the low-temperature regime to the high-temperature regime is given by eq 7, and values are listed in Table 1.

$$T_o = (\Delta H^{\ddagger}_{h} - \Delta H^{\ddagger}_{/})/(\Delta S^{\ddagger}_{h} - \Delta S^{\ddagger}_{/}) \quad (7)$$

Kinetics of the Association of NAD$^+$ with Tc-SAHH and Hs-SAHH. In contrast to the simple first-order reaction of cofactor dissociation, the association of NAD^+ with rat-liver SAHH has been reported (*18*) to exhibit biphasic kinetics, with half of the full complement of the cofactor binding during the dead time of the experiment and the other half binding over ~1 h (concentrations of apoenzyme of 15.9 μM and NAD^+ of 185−555 μM). Figure 3 shows the association kinetics for Tc-SAHH and Hs-SAHH for 1 μM apoenzyme (as monomers) reacting with 1−100 μM NAD^+ (further experiments, not shown, extended the range of NAD^+ concentrations to 300 μM). Both enzymes exhibit first-order kinetics of cofactor association at all cofactor concentrations, with the increase in enzyme activity A upon cofactor binding following eq 8, equivalent to eq 1 above, with A_o being the activity at the apparent time zero, A_f the activity at very long times, and k_{app} the first-order rate constant, all being functions of [NAD^+].

$$A = A_f - [(A_f - A_o)\exp(-k_{app}t)] \quad (8)$$

Particularly at cofactor concentrations greater than ~7 μM, considerable binding occurs during the mixing period or dead time of the experiment (fast binding) and is measured by A_o. The remainder of the sites is occupied more slowly with a rate constant k_{app} (slow binding) to produce a total final activity A_f which is the sum of activities generated by the fast-binding component and the slow-binding component.

A model to be presented in the Discussion suggests that the magnitudes of the fast-binding component of activity A_o, the sum of fast-binding and slow-binding components of activity A_f, and the rate constant k_{app} for the slow-binding

Table 1: Quasi-Thermodynamic Parameters of Activation and Conversion Temperatures[a,b] for Dissociation of NAD^+ from Hs-SAHH (30−37 °C) and Tc-SAHH (20−37 °C) at pH 7.4

enzyme	$\Delta S^{\ddagger}_{/}$ (J mol^{-1} K^{-1})	$\Delta H^{\ddagger}_{/}$ (kJ/mol)	$\Delta S^{\ddagger}_{h}$ (J mol^{-1} K^{-1})	$\Delta H^{\ddagger}_{h}$ (kJ/mol)	T_o (K)
Hs-SAHH	24 ± 1	116 ± 4	600 ± 25	297 ± 9	314 ± 21 (41 °C)
Tc-SAHH	170 ± 15	154 ± 8	610 ± 30	287 ± 8	302 ± 34 (29 °C)

[a] Values obtained from fits to eqs 6 and 7 of the data shown in Figure 2. [b] The temperature of intersection of the high-temperature and low-temperature limbs of the temperature dependence and thus the temperature of conversion between the two regimes.

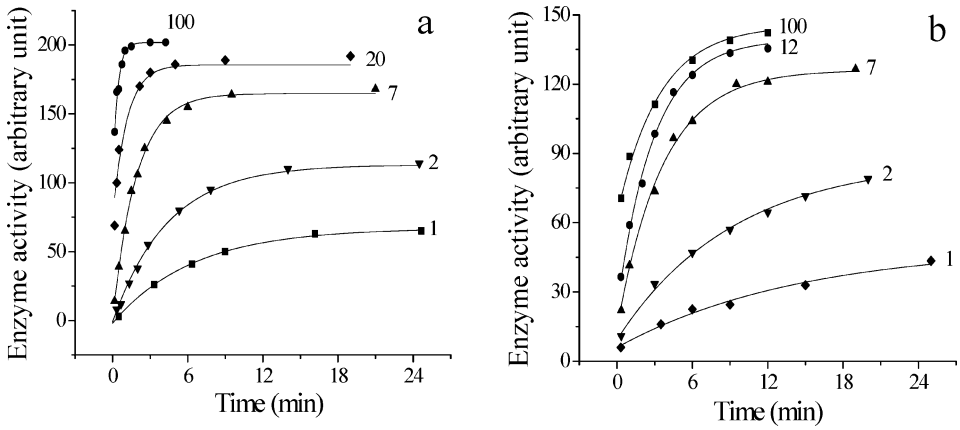

FIGURE 3: Time course of the increase in enzyme activity as NAD^+ associates with the apo forms of Hs-SAHH (a) and Tc-SAHH (b) at 23 °C and pH 7.4. In each case, representative curves are shown for low, medium, and high concentrations of NAD^+ (identified on the graphs by values of [NAD^+] in micromolar). The lines are plots of eq 8, with parameters A_o (the initial activity, reflecting the fast-binding component), A_f (the final activity, reflecting the sum of fast-binding and slow-binding components), and k_{app} (the rate constant for the slow-binding component), the values of which will be presented in subsequent figures. Note that all three parameters increase as [NAD^+] increases.

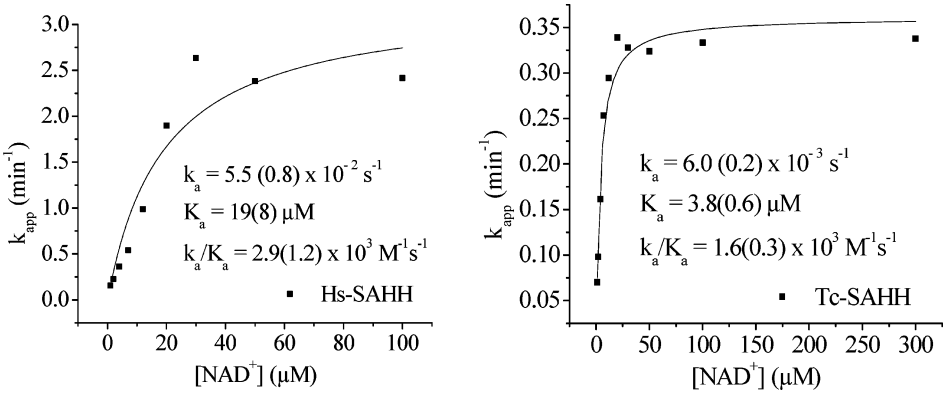

FIGURE 4: Dependence on the concentration of NAD^+ of the rate constants for the slow-binding phase of the association of NAD^+ with the apo forms of Hs-SAHH and Tc-SAHH at 23 °C and pH 7.4. Some obvious signs of cooperativity for Hs-SAHH have been neglected, and the data in both cases have been fitted to the simple hyperbolic saturation function of eq 9c. The parameters are shown in the figures with the standard deviations of fit in parentheses.

component of activity should depend on [NAD^+] according to eqs 9a−9c, respectively.

$$A_o = (A_t/2)[[NAD^+]^n/(K_o^n + [NAD^+]^n)] \quad (9a)$$

$$A_f = A_t[[NAD^+]/(K_f + [NAD^+])] \quad (9b)$$

$$k_{app} = k_a[[NAD^+]/(K_a + [NAD^+])] \quad (9c)$$

Here A_t is the total enzyme activity at a saturating NAD^+ concentration after completion of slow binding, k_a is the limiting rate constant for slow binding at a high NAD^+ concentration, n is a Hill coefficient needed to give an approximate account of apparent cooperativity, and K_o, K_f, and K_a are equilibrium dissociation constants for NAD^+ from three different forms of the active site (more detail is given in the Discussion). The data in Figure 4 were fit to eq 9c, resulting in the values of k_a and K_a shown in the figure.

The dependence of the rate constant k_{app} on cofactor concentration for the slow-binding reaction thus exhibits saturation above ~30 μM for both enzymes (Figure 4), consistent with the previous report for the rat liver enzyme (*19*) that the slow-binding rate constant is independent of cofactor concentration in the concentration range studied by those authors (185−555 μM). Furthermore, the affinities for NAD^+ of the various forms of the enzymes envisioned in the model described in the Discussion are sufficiently low

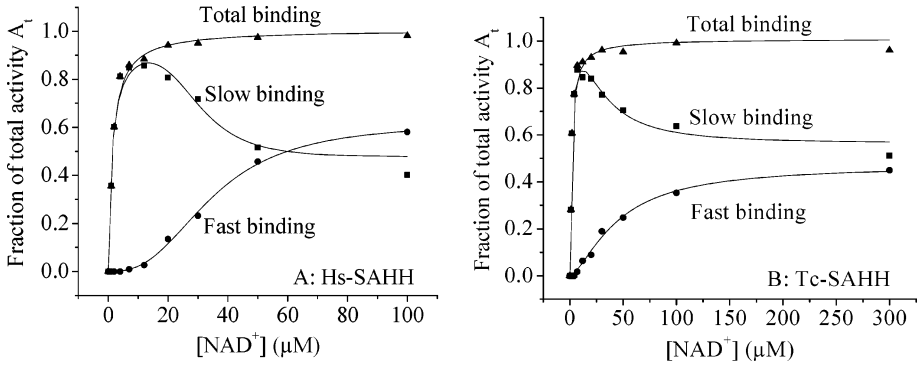

FIGURE 5: Dependence on [NAD$^+$] of the fractions of enzyme activity generated in the fast-binding phase (A_o in eq 8), the slow-binding phase ($A_f - A_o$ in eq 8), and the total activity (A_f in eq 8). The data were obtained in the kinetic experiments summarized in Figure 3, with those at the left (A) for Hs-SAHH and those at the right (B) for Tc-SAHH. For each enzyme, the data for fast binding, total binding, and slow binding were independently fitted to eq 9a, eq 9b, and eq 9b − eq 9a, respectively, to obtain the parameters given in the text. Equation 9a was used for fast binding in place of a hyperbolic function because of the distinctly sigmoid appearance of the data for Hs-SAHH; eq 9a was then also used for consistency in treating the data for Tc-SAHH, where the sigmoid character is less pronounced.

that even when the concentrations of the enzyme (monomers) and cofactor are equal at 1 μM, only ~20−25% of the monomers are occupied by the cofactor at the end of the experiment, so roughly first-order kinetics are observed in this case, and more rigorously as the concentration of cofactor increases (Figure 3).

Partition between Fast and Slow Binding of NAD$^+$ to Hs-SAHH and Tc-SAHH as a Function of [NAD$^+$]. Figure 5 shows the fractional activity produced in the fast-binding phase (as measured by A_o, the activity at the apparent zero of time), in the slow-binding phase (as measured by $A_f - A_o$), and the total fractional activity produced in both phases (A_f), all as a function of the cofactor concentration. The total fractional activity is saturated at close to unity in the range of 10−20 μM cofactor for both enzymes. The slow-binding reaction dominates at low cofactor concentrations, increasingly so until it accounts for ~80−85% of the total activity at ~10 μM cofactor for both enzymes. Thereafter, the fast-binding reaction increases in relative importance until the two processes each account for half the total activity above ~50 μM cofactor for Hs-SAHH and above ~300 μM cofactor for Tc-SAHH.

For Hs-SAHH, the fast-binding component shows extraordinary cooperativity as evidenced by the sigmoid appearance of the fast-binding curve in Figure 4. To account approximately for this characteristic, the Hill equation (eq 9a) was employed to fit the data in Figure 4. Slow binding was described by eq 9b − eq 9a. For total binding, the simple hyperbolic form of eq 9b was adequate and was therefore employed. Although the sigmoid character of the fast-binding curve for Tc-SAHH is less pronounced, the same three equations (eqs 9a−9c) were also used for these data.

For Hs-SAHH, the fast-binding data yield the following: $K_o = 35 \pm 1$ μM, $n = 2.7 \pm 0.2$, and $A_t = 1.27 \pm 0.04$. The total-binding data with n effectively fixed at 1.0 yield the following: $K_f = 1.4 \pm 0.1$ μM and $A_t = 1.01 \pm 0.02$. The slow-binding data yield the following: $K_o = 30 \pm 4$ μM, $K_f = 1.3 \pm 0.3$ μM, $n = 3.8 \pm 1.4$, and $A_t = 0.97 \pm 0.06$. For Tc-SAHH, the fast-binding data yield the following: $K_o = 45 \pm 4$ μM, $n = 1.5 \pm 0.1$, and $A_t = 0.94 \pm 0.04$. The total-binding data with n fixed at 1.0 yield the following: $K_f = 1.5 \pm 0.2$ μM and $A_t = 1.01 \pm 0.02$. The slow-binding data yield the following: $K_o = 31 \pm 9$ μM, $K_f = 2.0 \pm 0.4$ μM, $n = 1.7 \pm 0.4$, and $A_t = 1.13 \pm 0.09$. Mean values of the parameters are listed in Table 5.

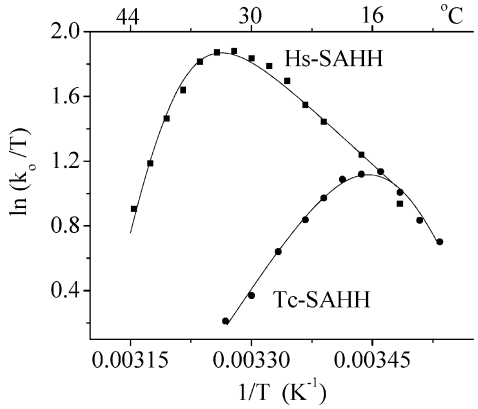

FIGURE 6: Temperature dependence of the rate constant for the slow-binding phase of the association of NAD$^+$ with the apo forms of Hs-SAHH (top curve) and Tc-SAHH (bottom curve). The lines are plots of eq 10 with the parameters listed in Table 2. The rate constants were obtained in kinetic experiments of the kind summarized in Figure 3.

Temperature Dependence of the Slow-Binding Kinetics of the Association of NAD$^+$ with Hs-SAHH and Tc-SAHH. The effect of temperature on the slow-binding rate constant for association of NAD$^+$ with Hs-SAHH and Tc-SAHH is shown by the Eyring plots in Figure 6. The rate was measured at 5 μM NAD$^+$, where the reaction is approximately first-order in the cofactor for both enzymes (see Figure 4), and the first-order rate constants k_{app} were divided by 5 μM to produce the second-order rate constants k_o that are plotted.

On the basis of a model, developed in more detail in the Discussion, in which a partial, reversible, and perhaps quite local unfolding at higher temperatures deprives both enzymes of the capacity to bind cofactor, the apparent second-order rate constant k_o for cofactor binding will be given by $k_{on}[1/(1 + K_{un})]$, where k_{on} is the second-order rate constant for binding of cofactor to the native form of the enzyme and the factor in parentheses is the fraction of enzyme in the native form, K_{un} being the equilibrium constant for the unfolding. The temperature dependence of the apparent association constant k_o will then be described by eq 10, where

Table 2: Thermodynamic and Quasi-Thermodynamic Parameters for Association of NAD^+ with Hs-SAHH and Tc-SAHH at Temperatures in the Interval of 11−45 °C

enzyme	$\Delta S^{\ddagger}_{on}$ ($J\ K^{-1}\ mol^{-1}$)	$\Delta H^{\ddagger}_{on}$ (kJ/mol)	ΔS°_{un} ($J\ K^{-1}\ mol^{-1}$)	ΔH°_{un} (kJ/mol)	$\Delta H^{\circ}_{un}/\Delta S^{\circ}_{un}$ (K)
Hs-SAHH	-56 ± 9	38 ± 3	788 ± 5	243 ± 2	308 ± 3 (35 °C)
Tc-SAHH	225 ± 13	118 ± 4	631 ± 8	182 ± 2	288 ± 5 (15 °C)

Table 3: Equilibrium Dissociation Constants for NAD^+ from Its Complexes with Hs-SAHH and Tc-SAHH at Temperatures from 30 to 37 °C

Hs-SAHH, $K_d^{NAD^+}$ (nM) [temp (°C)]	9.6 ± 0.4 (30 °C)	13 ± 1 (32 °C)	17 ± 1 (34 °C)	31 ± 3 (37 °C)	$\Delta H^{\circ} = 130 \pm 9$ kJ/mol; $\Delta S^{\circ} = 274 \pm 9\ J\ mol^{-1}\ K^{-1}$
Tc-SAHH, $K_d^{NAD^+}$ (μM) [temp (°C)]	0.63 ± 0.04 (30 °C)	2.1 ± 0.2 (32 °C)	5.7 ± 0.6 (34 °C)	19 ± 2 (37 °C)	$\Delta H^{\circ} = 378 \pm 24$ kJ/mol; $\Delta S^{\circ} = 1131 \pm 83\ J\ mol^{-1}\ K^{-1}$

we take the standard-state concentration of NAD^+, $[NAD^+]_{ss}$, to be 1 M:

$$\ln(k_o/T) = \Delta S^{\ddagger}_{on}/R - \Delta H^{\ddagger}_{on}/RT - \ln[1 + \exp(\Delta S^{\circ}_{un}/R - \Delta H^{\circ}_{un}/RT)] - \ln[NAD^+]_{ss} + \ln(k/h) \quad (10)$$

where the subscript on denotes the quasi-thermodynamic parameters of activation for cofactor binding and the subscript un denotes the thermodynamic parameters of the reversible unfolding process. The values of these quantities are given in Table 2. The table also gives the $\Delta H^{\circ}_{un}/\Delta S^{\circ}_{un}$ ratio, a rough measure of the "melting temperature" for the structural transition under observation.

Equilibrium Dissociation Constants for Dissociation of NAD^+ from Hs-SAHH and Tc-SAHH in the Temperature Range of 30−37 °C. From the k_{on} and k_{off} values at temperatures between 30 and 37 °C (Figures 2 and 6), equilibrium dissociation constants $K_d^{NAD^+}$ for NAD^+ were calculated for Hs-SAHH and Tc-SAHH (Table 3). The values are on the order of nanomolar for Hs-SAHH and micromolar for Tc-SAHH with the value of the $(K_d^{NAD^+})_{Tc}/(K_d^{NAD^+})_{Hs}$ ratio being ~600 at 37 °C. Table 3 also shows the values of enthalpies and entropies for dissociation of NAD^+ from the two enzymes.

Kinetics and Thermodynamics at 37 °C of the Association with and Dissociation from Tc-SAHH and Hs-SAHH of NADH. The equilibrium constants K_d^{NADH} for dissociation of NADH from its complexes with Hs-SAHH and Tc-SAHH were measured by competition between NAD^+ (with dissociation constants given in Table 3) and NADH, as described above. The values are 5.0 ± 0.1 nM for Hs-SAHH and 69 ± 6 nM for Tc-SAHH.

At NADH concentrations of <7 μM, the association rate with Hs-SAHH is first-order in NADH so that the rate constant k_{on} could be measured as $1940 \pm 90\ M^{-1}\ s^{-1}$ for Hs-SAHH and $930 \pm 90\ M^{-1}\ s^{-1}$ for Tc-SAHH.

The dissociation of NADH from Hs-SAHH is too slow to allow measurement of the rate constant for dissociation (k_{off}), but k_{off} can be computed from $K_d^{NADH}k_{on}$ as $(9.7 \pm 2.0) \times 10^{-6}\ s^{-1}$. A similar calculation for Tc-SAHH yields a value of $(64 \pm 10) \times 10^{-5}\ s^{-1}$, while a direct measurement, which is possible here, yields a value of $(69 \pm 6) \times 10^{-5}\ s^{-1}$.

Thermal Stability of the Apo Forms of Hs-SAHH and Tc-SAHH. Melting temperatures were determined by both DSC and CD for the thermal unfolding of the two proteins. The values for apo-Hs-SAHH are 44.9 ± 0.3 (DSC) and 44.2 ± 0.4 °C (CD) and for apo-Tc-SAHH are 53.0 ± 0.4 (DSC) and 52.8 ± 0.4 °C (CD). At temperatures below these values, apo-Hs-SAHH loses its capacity to bind NAD^+ (and thus become an active catalyst) more rapidly than does apo-Tc-SAHH (at 22 °C, Hs-SAHH loses this capacity completely within 30 h, while Tc-SAHH still retains half of its capacity at 90 h).

Table 4: Rate and Equilibrium Constants for the Association and Dissociation of S-NAD^+ and S-NADH with Hs-SAHH and Tc-SAHH at 37 °C

enzyme	ligand	k_{on}[a] ($M^{-1}\ s^{-1}$)	k_{off} ($\times 10^6\ s^{-1}$)	K_d (nM)
Hs-SAHH	S-NAD^+	4153 ± 303	162 ± 11	39 ± 1
	S-NADH	4000 ± 712	148 ± 26	37 ± 1
Tc-SAHH	S-NAD^+	356 ± 29	5450 ± 300	15300 ± 9000
	S-NADH	467 ± 59	304 ± 26	651 ± 60

[a] Calculated as k_{off}/K_d.

Evaluation of the NAD^+ and NADH Analogues S-NAD^+ and S-NADH as Selective Inhibitors for Hs-SAHH and Tc-SAHH. S-NAD^+ and S-NADH, the side chain thione analogues of the natural cofactors, were tested for their ability to inhibit AdoHcy hydrolase activity. Hs-SAHH and Tc-SAHH, reconstituted with S-NAD^+, exhibit ~1% of the activity of the NAD^+ form, and the S-NADH forms of both enzymes exhibit no measurable activity. The association and dissociation rate constants and equilibrium dissociation constants for S-NAD^+ and S-NADH with Hs-SAHH and Tc-SAHH at 37 °C are summarized in Table 4. As a test of the relative efficacy of these substances as inhibitors of Hs-SAHH and Tc-SAHH, the enzymes (both in their active NAD^+ forms) were exposed to 50 μM S-NAD^+ or 20 μM S-NADH in the presence of 50 μM NAD^+ to simulate roughly the estimated (*19*) 70 μM levels of NAD^+ *in vivo* (Figure 5). Hs-SAHH was affected very little (2% inhibition with each inhibitor) in the first 5 min, during which Tc-SAHH lost 45% of its activity with S-NAD^+ or 52% with S-NADH. An apparent equilibrium was reached for Tc-SAHH after exposure for 10−20 min with all activity lost in the presence of S-NADH and approximately half lost in the presence of S-NAD^+. The apparent equilibrium for Hs-SAHH is reached after incubation for only 12 h.

DISCUSSION

Kinetics of the Dissociation of NAD^+ from Hs-SAHH and Tc-SAHH. The data presented in Figure 1 and Table 1 show that the dissociation of 4 equiv of NAD^+ from the four active sites of homotetrameric SAHH proceeds by a simple first-order reaction, making no distinction in the rate of dissociation among the four active sites. The loss of cofactor thus exhibits no apparent cooperativity. The rate constants for

dissociation are substantially larger for Tc-SAHH than for Hs-SAHH; for example, at 37 °C, dissociation from Tc-SAHH is approximately 90-fold faster (legend of Figure 1).

Temperature Dependence of the Kinetics of the Dissociation of NAD$^+$ from Tc-SAHH and Hs-SAHH. Figure 2 shows that the rate constants of NAD$^+$ dissociation in the cases of both Hs-SAHH and Tc-SAHH generate nonlinear Eyring plots. The upward curvature or "bowl shape" of these two plots can arise from a number of sources. The possible explanations are not always practically or even theoretically distinguishable, but a reasonable hypothesis would be that a structural change in the enzyme as the temperature is changed affects the activation parameters for the dissociation reaction. Attempts to describe the temperature dependence simply by two parallel routes of dissociation with different activation parameters were unsuccessful. The data are too sparse to evaluate in detail the hypothesis of a thermally induced structural transition, but some comments on the activation parameters in the high-temperature and low-temperature regimes can be made.

As Table 1 shows, the value of $\Delta H^{\ddagger}$ along the low-temperature limb of the Eyring plots is 116 kJ/mol for Hs-SAHH and 154 kJ/mol for Tc-SAHH, so if entropic contributions were equal, the cofactor would dissociate from Hs-SAHH 4×10^6-fold faster than from Tc-SAHH at 300 K. In fact, the values of $\Delta S^{\ddagger}$ along the low-temperature limb of the Eyring plots are 24 J mol^{-1} K^{-1} for Hs-SAHH and 170 J mol^{-1} K^{-1} for Tc-SAHH, a difference that, taken alone, would confer a rate advantage of 4×10^7-fold on dissociation from Tc-SAHH over Hs-SAHH. The entropic contribution thus more than overcomes the enthalpic contribution so that dissociation of NAD$^+$ from Tc-SAHH is faster than that from Hs-SAHH by roughly 10-fold in the low-temperature regime.

Along the high-temperature limb of the Eyring plots, the values of $\Delta H^{\ddagger}$ and $\Delta S^{\ddagger}$ for the two enzymes are within experimental error of each other (but note the long extrapolation of a few points to obtain the values). Phenomenologically, dissociation from Tc-SAHH occurs more rapidly than from Hs-SAHH by factors in the range of 10−100-fold, and indeed, the mean values of both $\Delta H^{\ddagger}$ and $\Delta S^{\ddagger}$ favor a more rapid dissociation from Tc-SAHH by factors in this range. One feature of the data is that the conversion temperature between the thermal regimes, which is given by eq 7 above, is considerably higher for Hs-SAHH (∼41 °C) than for Tc-SAHH (∼29 °C). The result is that at 37 °C, Tc-SAHH has entered the high-temperature regime and the rate constant has been increasing rapidly with temperature while Hs-SAHH remains in the low-temperature regime, where the rate constant is not increased as much by the increasing temperature. At 37 °C then, dissociation from Tc-SAHH is ∼90-fold faster than from Hs-SAHH.

The large increase in the values of the entropies of activation for dissociation of NAD$^+$ from both enzymes as the temperature increases through the range of 30−40 °C may suggest that the faster dissociation rates at higher temperatures derive in part from an increased mobility in the apoenzyme of the unoccupied binding site for NAD$^+$. The fact that the conversion temperature is lower for Tc-SAHH would then suggest that the ease with which the increased mobility can be thermally induced is greater for Tc-SAHH.

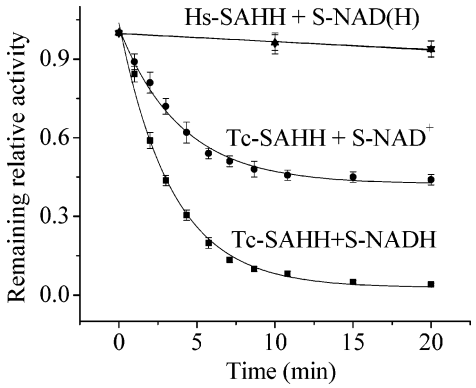

FIGURE 7: Loss of activity of Hs-SAHH (top curve, for 50 μM S-NAD$^+$ and for 20 μM S-NADH) and of Tc-SAHH (middle curve, 50 μM S-NAD$^+$, and bottom curve, 20 μM S-NADH) in solutions containing 4 μM enzyme and 50 μM NAD$^+$ at 37 °C and pH 7.4. Errors were calculated from two independent measurements.

Observed Kinetics of the Association of NAD$^+$ with Tc-SAHH and Hs-SAHH. The association process, in contrast to the dissociation process, appears kinetically complicated, as shown in Figures 3−5. The association processes for Hs-SAHH and Tc-SAHH exhibit qualitatively similar but quantitatively different characteristics, as measured by the appearance of enzyme activity when NAD$^+$ becomes bound in the active sites.

For each enzyme, there is a fraction of occupation A_o of the total binding that occurs during the dead time of the experiment and depends in a saturating manner on [NAD$^+$]. A first-order time-dependent fraction of binding with rate constant k_{app} then follows, and k_{app} also depends in a saturating manner on [NAD$^+$]. The total fraction of binding A_f at the end of the slow-binding phase depends in a saturating manner on [NAD$^+$] and corresponds to full occupancy of all active sites at high cofactor concentrations. All three kinetic parameters of binding, A_o, A_f, and k_{app}, thus exhibit saturation behavior with cofactor concentration, but the half-saturation concentrations of the cofactor are different in each case (Figures 4 and 5).

Figure 5 also shows that the fraction of activity generated by the slow-binding phenomenon ($A_f - A_o$) exhibits a particularly complex dependence on [NAD$^+$]. At low NAD$^+$ concentrations, the slow-binding fraction increases sharply until it accounts for more than 80% of the total binding. Thereafter, it falls as the fast-binding fraction increases until at high NAD$^+$ concentrations (>60 μM for Hs-SAHH and >200 μM for Tc-SAHH), both the slow-binding and fast-binding phenomena account for roughly half of the enzyme activity.

A Model for the Kinetics of Association of NAD$^+$ with Hs-SAHH and Tc-SAHH. A model that accommodates these observations is depicted in Figure 8. Its basic assumption is that apo-SAHH from both species, before exposure to cofactor, contains two equally populated classes of active sites. Upon introduction of cofactor, all sites can and do bind NAD$^+$ rapidly; however, in one class of sites (dissociation constant K_o), binding of NAD$^+$ generates a fully functional active site, while in the other class of sites (dissociation constant K_a), binding of NAD$^+$ generates no enzyme activity. Thus, the initial activity A_o (see Figures 3−5 and eqs 9 above) is given by the total population of potentially functional sites (A_t/2) multiplied by the fraction of these sites

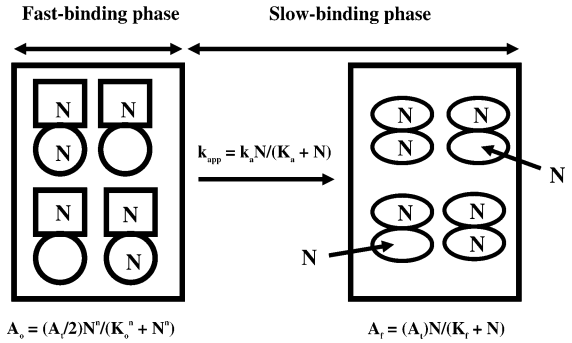

FIGURE 8: Speculative model for association and time-dependent activation of apo-SAHH by binding of NAD^+. The tetrameric apoenzyme molecule is assumed to contain two classes of binding sites in equal amounts, the molecule thus being represented by a square−circle shape. The box at the left represents the situation during the fast-binding phase. Upon introduction of the cofactor, represented by the letter N, both classes of sites are assumed to become wholly or partially occupied as shown in the box at the left. The circle sites are assigned a cofactor dissociation constant K_o and are assumed to be fully capable of catalysis when occupied. The square sites are assigned a cofactor dissociation constant K_a, and they are assumed to be incapable of catalysis whether they are occupied by N or not. Equilibration of binding occurs within the dead time of the experiment and constitutes the fast phase of generation of catalytic activity, which arises solely from the occupied circle sites. The initial activity is then equal to A_o as shown below the box at the left. The box at the right represents the situation following the slow-binding phase. During the slow phase, those species that contain N bound into a square site undergo a reorganization in which the occupied square site and the adjacent circle site, whether it is occupied or not, are converted to oval sites as shown at the right. Oval sites have the same catalytic activity as circle sites, but their substrate affinity is greater so that, as shown, more sites are rapidly occupied, as they become oval sites. The reorganization is driven by the fraction of occupied square sites, thus occurring with rate constant $k_aN/(K_a + N)$. Because the reorganization is irreversible, the entirety of the enzyme will be converted during the slow phase. The resulting enzyme equilibrates rapidly with free N, with all sites now having a dissociation constant K_f. The final activity is then given by the expression shown below the box at the right. The three equations in the figure are eqs 9a−9c of the text.

occupied at a given $[NAD^+] = N$, i.e., $N^n/(K_o^n + N^n)$. The Hill equation formalism allows for the sigmoid character of the N dependence of A_o visible in Figure 5. In Figure 8, the initial situation is portrayed by the left-hand box and the expression for A_o is given below the box.

Binding at the nonfunctional sites, although tighter than that to the potentially functional sites, generates no activity. Binding of the cofactor in such a site does, however, initiate a time-dependent process (rate constant k_a) in which the nonfunctional sites, occupied to a fractional extent $[N/(K_a + N)]$ of their total, are transformed—along with their partner sites whether the latter are occupied or not—into pairs of active sites both of which are potentially fully catalytically active when occupied by cofactor. This slow-binding phase leads to a functionally homotetrameric enzyme with an equilibrium constant K_f for dissociation of NAD^+ from any of the active sites. This form of the enzyme is in rapid, reversible cofactor binding equilibrium at all active sites.

The situation at the end of the slow-binding phase is represented in Figure 8 by the box on the right-hand side. Since binding at all sites is now rapid and reversible and because (a) $K_f < K_a < K_o$ so that all sites at the end of the slow phase have greater cofactor affinity than any site before the slow phase and (b) the slow phase leads to the generation of two potentially functional sites of high affinity where only the nonfunctional partner was occupied initially, the overshoot phenomenon results at low cofactor levels. At low NAD^+ levels, the occupancy of the initially functional sites is low (especially as a consequence of the cooperativity in their occupation), and the occupancy of nonfunctional sites is relatively high. The highly occupied nonfunctional sites then transform along with their partner sites into fully functional sites of still higher affinity. These factors combine to generate the overshoot characteristic.

The expression over the arrow describes the N dependence of k_{app} (Figure 4), and the expression below the right-hand box describes the N dependence of A_f (Figure 5).

The values of the parameters of the model, as understood from Figure 8 and eqs 9, are given in Table 5. The values were obtained by fitting of the data of Figures 3−5 to eqs 9 as described in the Results.

To put into quantitative terms the description given above, fast binding of NAD^+ within the dead time of the experiment to potentially functional sites from which the dissociation constant K_o is 33 μM (Hs-SAHH) or 38 μM (Tc-SAHH) occurs. At the same time, sites with no catalytic capacity but greater affinity ($K_a = 19$ μM for Hs-SAHH and $\sim$4 μM for Tc-SAHH) are rapidly occupied. A time-dependent conversion of these sites (and their partner sites whether they are occupied or not) to fully active sites then ensues (k_a $\sim$10-fold larger for Hs-SAHH and corresponding to characteristic times of $\sim$20 s for Hs-SAHH and 3 min for Tc-SAHH). At the end of the time-dependent phase, all active sites have the same activity and dissociation constant (1.4−1.5 μM for both enzymes).

The qualitative character of the cofactor association process is the same for both enzymes, and some quantitative features are similar. For example, the nonfunctional sites of the apoenzyme bind cofactor approximately twice as tightly as the functional active sites for Hs-SAHH and 10-fold as tightly for Tc-SAHH. This feature contributes to the overshoot of the slow-binding reaction (Figure 5), because more of the nonfunctional than the functional sites are initially occupied. More important, however, is the fact that each occupied nonfunctional site leads to two functional sites of high affinity in the final enzyme, and thus, the slow phase comes to account for 80−85% of the final activity at NAD^+ concentrations below the saturation values for the functional active sites.

These qualitative features apply to both enzymes, but quantitative distinctions exist. The achievement of final full activity occurs $\sim$10 times faster for Hs-SAHH, as already noted. Furthermore, the rates of cofactor dissociation are quite different for the two enzymes, as will be discussed below, and both of these distinctions may be of some importance.

It should be noted as well that the values of K_f, the apparent dissociation constants of NAD^+ corresponding to a period $\sim$30−60 min after mixing of apoenzymes with cofactor, are on the order of 1−2 μM (23 °C) for both Hs-SAHH and Tc-SAHH (Table 5). When the dissociation constants of NAD^+ are instead calculated as the ratio of dissociation and association rate constants, the dissociation rate constants obtained from fully reconstituted enzyme that has not only completed both phases of binding but also

Table 5: Values of Rate and Equilibrium Constants in the Kinetics of the Fast- and Slow-Binding Phases of the Association Reaction of NAD^+ with Hs-SAHH and Tc-SAHH at 23 °C and pH 7.4, According to the Model in Figure 8

enzyme	K_o (μM), binding to fully functional sites of apo-SAHH	K_a (μM), binding to nonfunctional sites of apo-SAHH	K_f (μM), binding to fully functional sites of holo-SAHH	k_a (s^{-1}), transformation of apo sites to functional holo sites	k_a/K_a (M^{-1} s^{-1}), binding and transformation of apo sites to holo sites
Hs-SAHH	33 ± 4 ($n = 3.3 \pm 1.4$)	19 ± 8	1.4 ± 0.3	$(5.5 \pm 0.8) \times 10^{-2}$	$(2.9 \pm 1.2) \times 10^3$
Tc-SAHH	38 ± 9 ($n = 1.6 \pm 0.4$)	3.8 ± 0.6	1.8 ± 0.4	$(6.0 \pm 0.2) \times 10^{-3}$	$(1.6 \pm 0.3) \times 10^3$

thereafter undergone further maturation for hours or more, $K_d^{NAD^+}$ for Tc-SAHH remains approximately the same [0.6 μM at 30 °C (Table 3)]. In contrast, the $K_d^{NAD^+}$ for Hs-SAHH is around 10 nM at 30 °C, roughly 100-fold smaller than K_f. These results seem to indicate that the loose binding observed for Tc-SAHH after 30−60 min persists and represents the final thermodynamic equilibrium binding, while with Hs-SAHH, a further change in the strength of binding occurs over some hours, resulting in a further 100-fold increase in the strength of association of the cofactor with Hs-SAHH.

Temperature Dependence of the Slow-Binding Kinetics of the Association of NAD^+ with Hs-SAHH and Tc-SAHH. The data in Figure 6 were obtained at 5 μM NAD^+ so that for Hs-SAHH [$K_a = 19$ μM at 23 °C (Table 5)] the apparent second-order rate constant k_o is roughly equal to k_a/K_a, a constant similar to k_{cat}/K_M in enzyme catalysis. For Tc-SAHH [$K_a = 4$ μM at 23 °C (Table 5)], the situation is not so simple; the phenomenological observation that k_o in the neighborhood of 5 μM NAD^+ remains proportional to [NAD^+] for Tc-SAHH leads us to treat it as being roughly equal to k_a/K_a. Figure 6 shows that at low temperatures the observed k_o is approximately the same for the two enzymes. Extrapolating to 23 °C gives a value near 1500 M^{-1} s^{-1}, not so different from k_a/K_a [2900 M^{-1} s^{-1} for Hs-SAHH and 1600 M^{-1} s^{-1} for Tc-SAHH (Table 5)].

As already noted, the "dome-shaped" temperature dependences in Figure 6 can arise from a model in which increasing temperature on the one hand increases the value of the rate constant k_a/K_a while at the same time increasing the fraction of protein that has undergone an at least partial, reversible unfolding to a form that can no longer bind the cofactor {equilibrium constant K_{un} so that, as above, $k_o = k_{on}[1/(1 + K_{un})]$} with k_{on} being approximately equal to k_a/K_a.

As can be seen in both Figure 6 and Table 2, the quasi-thermodynamic parameters of activation for k_{on} are different for Hs-SAHH and Tc-SAHH. The values of $\Delta H^{\ddagger}$ are approximately 38 and 118 kJ/mol, respectively, and the values of $\Delta S^{\ddagger}$ are approximately −56 and 225 J mol^{-1} K^{-1}, respectively. The low-temperature limbs of the temperature dependences for the two enzymes do nearly superimpose, but only because the enzyme with the more favorable enthalpy of activation (Hs-SAHH) also has the less favorable entropy of activation. The combination of a small enthalpic barrier with a negative entropy of activation for Hs-SAHH would be consistent with a transition state for Hs-SAHH that comes after the development of a considerable part of the binding interactions between the cofactor and protein (low enthalpy from liberation of binding energy, negative entropy from rigidification of segments of protein and cofactor structures). The combination of a larger enthalpic barrier with a positive entropy of activation for Tc-SAHH would be consistent with a transition state for Tc-SAHH that comes at a point where desolvation of the cofactor has advanced to some degree (thus, high enthalpy from loss of solvation energy, positive entropy from liberation of water molecules); however, few protein−cofactor interactions have developed, and thus, the liberation of binding energy and rigidification of structure cannot cancel the contributions just described.

The thermodynamic values for the equilibrium constant of the postulated unfolding phenomenon are not extremely different for Hs-SAHH and Tc-SAHH [$\Delta H°_{un} \sim 243$ and 182 kJ/mol, respectively, and $\Delta S°_{un} \sim 788$ and 631 J mol^{-1} K^{-1}, respectively (Table 2)]. The ratios $\Delta H°_{un}/\Delta S°_{un}$ of these values lead to "melting" temperatures for the corresponding unfolding process of 35 (Hs-SAHH) and 15 °C (Tc-SAHH), not far from the temperatures at which the two Eyring plots exhibit maxima [34 °C for Hs-SAHH and 17 °C for Tc-SAHH (Figure 6)]. It should be noted that this melting does not correspond to global unfolding of the enzymes, which occurs around 44−45 (Hs-SAHH) and 52−53 °C (Tc-SAHH). This suggests a more local phenomenon is adversely affecting the capacity of the enzyme to bind the cofactor.

The maxima are not expected to occur at the global melting temperatures but rather at the temperature for which the local unfolding process begins to dominate the rate process in determining the value of k_o, i.e., the temperature T_{max} for which $d[\ln(k_o/T)]/d(1/T) = 0$. From this requirement, it emerges that at T_{max}, the fraction of locally unfolded protein $K_{un}^{max}/(1 + K_{un}^{max}) = \Delta H^{\ddagger}_{on}/\Delta H°_{un}$. This fraction is 0.19 for Hs-SAHH and 0.61 for Tc-SAHH, yielding K_{max} values of 0.23 (Hs-SAHH) and 1.6 (Tc-SAHH), whence T_{max} {$=\Delta H°_{un}/[\Delta S°_{un} - R \ln(K_{max})]$} is found to be 34 (Hs-SAHH) and 16 °C (Tc-SAHH), in good agreement with the observed values of 34 °C for Hs-SAHH and 17 °C for Tc-SAHH.

Equilibrium Dissociation Constants for Dissociation of NAD^+ from Hs-SAHH and Tc-SAHH in the Temperature Range of 30−37 °C. In this limited temperature range where the on-rate constants and off-rate constants for both enzymes exhibit linear Eyring plots, effective equilibrium dissociation constants can be calculated for NAD^+ (Table 3). They are substantially larger for Tc-SAHH than for Hs-SAHH, the ratio ranging from 66 at the low end to 613 at the high end of the temperature range. The lower relative affinity of Tc-SAHH for the oxidized cofactor derives from the cancellation of enthalpic and entropic factors. There is a much greater enthalpy cost for dissociation from Tc-SAHH (greater by 248 ± 25 kJ/mol), but this is combined with a larger entropic advantage for dissociation of NAD^+ from Tc-SAHH (greater by 263 ± 25 J mol^{-1} K^{-1}). The increased affinity of several hundred-fold shown by Hs-SAHH thus arises from this cancellation of two very large and opposite contributions.

For both enzymes, the enthalpy of dissociation of NAD^+ is positive and the entropy of dissociation of NAD^+ is positive. This result is expected for the enthalpy because the attractive interactions of the cofactor with its binding site must be ruptured upon dissociation. The observed result is

also expected for the entropy because two particles are generated from one (a minor contribution) and because rupture of the binding interactions allows increased freedom of motion within both cofactor and enzyme molecules. One interpretation of the much larger values of both the enthalpy and entropy terms for Tc-SAHH than for Hs-SAHH would be that a substantially greater mobility of the unoccupied cofactor-binding site in apo-TcSAHH would require a larger entropy loss to fix in place the enzyme structural elements that bind to the cofactor (thus a larger entropy gain on dissociation) but that the same mobility would permit the development of a more favorable set of binding interactions, producing a larger release of energy upon binding and a larger energy cost for dissociation. This subject will be addressed in later papers in this series.

Kinetics and Thermodynamics at 37 °C of the Association of NADH with and Dissociation of NADH from Tc-SAHH and Hs-SAHH. The association rate constant for NADH is approximately twice as large for Hs-SAHH (1940 M^{-1} s^{-1}) as for Tc-SAHH (930 M^{-1} s^{-1}), while the dissociation rate constant is smaller by ~6-fold, resulting in a lower affinity of NADH for Tc-SAHH than for Hs-SAHH by ~14-fold. This difference is somewhat smaller than that for NAD^+ (600-fold tighter with Hs-SAHH), which results from the fact that the affinity of Hs-SAHH for cofactor is roughly the same whether the cofactor is oxidized or reduced (in the range of nanomolar in both cases), while the affinity of Tc-SAHH for cofactor is much greater for the reduced form (a bit over nanomolar) than for the oxidized form (roughly micromolar).

Thermal Stability of the Apo Forms of Hs-SAHH and Tc-SAHH. As already mentioned, the global unfolding of apo-Hs-SAHH occurs at a temperature approximately 10 °C lower than that for apo-Tc-SAHH. Combined with the observations above that the two enzymes have differing affinities for both oxidized and reduced cofactors, and that in the case of the oxidized cofactor, these difference arise from large and opposing differences in enthalpies and entropies of association and dissociation, the difference in overall thermal stability favoring Tc-SAHH may signal differences in the dynamics of the cofactor binding sites. Since we can detect no structural differences in this region of the enzymes (unpublished data, which refer to the enzyme with NADH and oxidized substrate analogue as ligands), the dynamical differences may allow the nucleation of the global unfolding process in the cofactor-binding region, at a temperature lower for Hs-SAHH than for Tc-SAHH. This could reflect a greater thermal mobility for the cofactor site in Hs-SAHH, allowing it to adapt to the cofactor as it binds, leading to stronger affinity. This would conflict, however, with the larger entropy of dissociation shown by Tc-SAHH, so the matter is almost certainly more complicated than this view.

Evaluation of the NAD^+ and NADH Analogues S-NAD^+ and S-NADH as Selective Inhibitors for Hs-SAHH and Tc-SAHH. The comparative inhibitory effect of S-NAD^+ and S-NADH on Hs-SAHH and Tc-SAHH (Figure 7 and Table 4) does not depend only on their relative affinity for the two enzymes, which is nearly 400-fold greater for Hs-SAHH in the case of S-NAD^+ and nearly 20 times greater for Hs-SAHH in the case of S-NADH. Instead, the major factor is the exposure of an empty cofactor binding site to the environment, which occurs by dissociation of NAD^+ with a rate constant at 37 °C for Hs-SAHH of 5.8×10^{-5} s^{-1} and for Tc-SAHH of 4.7×10^{-3} s^{-1}, a factor (as noted above) that is ~90-fold faster for Tc-SAHH. The exposed site is then competitively trapped by the inhibitor and the cofactor. The dissociation is probably the rate-limiting step, and the half-life of dissociation (~2.5 min from Figure 2) should match the half-life of inhibitor binding as is found, the latter being (Figure 7) ~2.5 min for binding of both S-NAD^+ and S-NADH. As Figure 7 shows, the difference between the two inhibitors is the fact that S-NADH is capable of displacing NAD^+ and generating complete loss of activity. This is consistent with the substantially greater affinity of Tc-SAHH for S-NADH than for S-NAD^+ (nearly 25-fold from Table 4).

These data thus suggest that the faster off-rate of cofactor with Tc-SAHH could be exploited in the design of inhibitors that bind rapidly to the cofactor site of Tc-SAHH but only far more slowly to Hs-SAHH. Such inhibitors could be highly selective for the parasitic enzyme on the basis of the kinetic properties of the parasitic and human enzymes even if, as seen here, the human enzyme has a much larger equilibrium affinity for the inhibitor (greater by 400-fold in this case).

Conclusions. The equilibrium and kinetic properties of association and dissociation of the cofactor by Hs-SAHH and Tc-SAHH are qualitatively similar. Both enzymes bind NAD^+ in a complex scheme that behaves as if the apoenzyme has two numerically equal classes of sites that bind cofactor and generate catalytic activity either very rapidly (<1 min) or quite slowly (>30 min). NAD^+ dissociates from all four sites of both enzymes in a single first-order reaction. Both enzymes exhibit the "dimer of dimers" structure (*1*, *11*; unpublished data of Q.-S. Li and W. Huang) in which the homotetramer is made up of two pairs of monomers, and within each pair of monomers, a C-terminal segment from each partner penetrates into the other partner subunit and forms part of the cofactor binding site. These two communicating active sites may thus correspond to the two classes of active sites required in the kinetic model for binding cofactor that is discussed above.

The quantitative properties for cofactor association and dissociation of Hs-SAHH and Tc-SAHH are very different. The equilibrium affinities of Hs-SAHH for NAD^+ and NADH are both in the nanomolar range, while the equilibrium affinity of Tc-SAHH for NAD^+ is in the micromolar range and its affinity for NADH in the nanomolar range, not far from the affinity of Hs-SAHH for NADH. The slow binding of NAD^+ by both enzymes exhibits saturation kinetics with respect to the cofactor concentration; however, binding to Hs-SAHH has a maximum rate constant of ~0.06 s^{-1}, while the rate constant for binding to Tc-SAHH levels out at 0.006 s^{-1}.

The dissociation rate constants for NAD^+ show a complex temperature dependence with both enzymes, but the cofactor always dissociates more rapidly from Tc-SAHH than from Hs-SAHH, the ratio being around 80-fold at 37 °C. This feature presents an opening for selective inhibition of Tc-SAHH over Hs-SAHH, demonstrated with the thioamide analogues of NAD^+ and NADH, which inactivated Tc-SAHH 60% (NAD^+ analogue) or 100% (NADH analogue) within 30 min, while the level of inhibition of Hs-SAHH

approached 30% only after 12 h. The following papers in this series will present information that illuminates the structural features of Hs-SAHH and Tc-SAHH that are responsible for these differences.

REFERENCES

1. Turner, M. A., Yang, X., Yin, D., Kuczera, K., Borchardt, R. T., and Howell, P. L. (2000) Structure and function of S-adenosylhomocysteine hydrolase, *Cell Biochem. Biophys. 33*, 101−125.
2. Chiang, P. K. (1998) Biological effects of inhibitors of S-adenosylhomocysteine hydrolase, *Pharmacol. Ther. 77*, 115−134.
3. Parker, N. B., Yang, X., Hanke, J., Mason, K. A., Schowen, R. L., Borchardt, R. T., and Yin, D. H. (2003) *Trypanosoma cruzi*: Molecular cloning and characterization of the S-adenosylhomocysteine hydrolase, *Exp. Parasitol. 105*, 149−158.
4. Yang, X., and Borchardt, R. T. (2000) Overexpression, purification, and characterization of S-adenosylhomocysteine hydrolase from *Leishmania donovani*, *Arch. Biochem. Biophys. 383*, 272−280.
5. Creedon, K. A., Rathod, P. K., and Wellems, T. E. (1994) *Plasmodium falciparum* S-adenosylhomocysteine hydrolase. cDNA identification, predicted protein sequence, and expression in *Escherichia coli*, *J. Biol. Chem. 269*, 16364−16370.
6. Henderson, D. M., Hanson, S., Allen, T., Wilson, K., Coulter-Karis, D. E., Greenberg, M. L., Hershfield, M. S., and Ullman, B. (1992) Cloning of the gene encoding *Leishmania donovani* S-adenosylhomocysteine hydrolase, a potential target for antiparasitic chemotherapy, *Mol. Biochem. Parasitol. 53*, 169−183.
7. Whaun, J. M., Miura, G. A., Brown, N. D., Gordon, R. K., and Chiang, P. K. (1986) Antimalarial activity of neplanocin A with perturbations in the metabolism of purines, polyamines and S-adenosylmethionine, *J. Pharmacol. Exp. Ther. 236*, 277−283.
8. Bitonti, A. J., Baumann, R. J., Jarvi, E. T., McCarthy, J. R., and McCann, P. P. (1990) Antimalarial activity of a 4′,5′-unsaturated 5′-fluoroadenosine mechanism-based inhibitor of S-adenosyl-L-homocysteine hydrolase, *Biochem. Pharmacol. 40*, 601−606.
9. Seley, K. L., Schneller, S. W., De Clercq, E., Rattendi, D., Lane, S., Bacchi, C. J., and Korba, B. (1998) The importance of the 4′-hydroxyl hydrogen for the anti-trypanosomal and antiviral properties of (+)-5′-noraristeromycin and two 7-deaza analogues, *Bioorg. Med. Chem. 6*, 797−801.
10. Nakajima-Shimada, J., Hirota, Y., and Aoki, T. (1996) Inhibition of *Trypanosoma cruzi* growth in mammalian cells by purine and pyrimidine analogs, *Antimicrob. Agents Chemother. 40*, 2455−2458.
11. Turner, M. A., Yuan, C. S., Borchardt, R. T., Hershfield, M. S., Smith, G. D., and Howell, P. L. (1998) Structure determination of selenomethionyl S-adenosylhomocysteine hydrolase using data at a single wavelength, *Nat. Struct. Biol. 5*, 369−376.
12. Hu, Y., Komoto, J., Huang, Y., Gomi, T., Ogawa, H., Takata, Y., Fujioka, M., and Takusagawa, F. (1999) Crystal structure of S-adenosylhomocysteine hydrolase from rat liver, *Biochemistry 38*, 8323−8333.
13. Tanaka, N., Nakanishi, M., Kusakabe, Y., Shiraiwa, K., Yabe, S., Ito, Y., Kitade, Y., and Nakamura, K. T. (2004) Crystal structure of S-adenosyl-L-homocysteine hydrolase from the human malaria parasite *Plasmodium falciparum*, *J. Mol. Biol. 343*, 1007−1017.
14. Yang, X., Hu, Y., Yin, D. H., Turner, M. A., Wang, M., Borchardt, R. T., Howell, P. L., Kuczera, K., and Schowen, R. L. (2003) Catalytic strategy of S-adenosyl-L-homocysteine hydrolase: Transition-state stabilization and the avoidance of abortive reactions, *Biochemistry 42*, 1900−1909.
15. Huang, Y., Komoto, J., Takata, Y., Powell, D. R., Gomi, T., Ogawa, H., Fujioka, M., and Takusagawa, F. (2002) Inhibition of S-adenosylhomocysteine hydrolase by acyclic sugar adenosine analogue D-eritadenine. Crystal structure of S-adenosylhomocysteine hydrolase complexed with D-eritadenine, *J. Biol. Chem. 277*, 7477−7482.
16. Yuan, C. S., Yeh, J., Liu, S., and Borchardt, R. T. (1993) Mechanism of inactivation of S-adenosylhomocysteine hydrolase by (*Z*)-4′,5′-didehydro-5′-deoxy-5′-fluoroadenosine, *J. Biol. Chem. 268*, 17030−17037.
17. Yuan, C. S., Ault-Riche, D. B., and Borchardt, R. T. (1996) Chemical modification and site-directed mutagenesis of cysteine residues in human placental S-adenosylhomocysteine hydrolase, *J. Biol. Chem. 271*, 28009−28016.
18. Gomi, T., Takata, Y., and Fujioka, M. (1989) Rat liver S-adenosylhomocysteinase. Spectrophotometric study of coenzyme binding, *Biochim. Biophys. Acta 994*, 172−179.
19. Fjeld, C. C., Birdsong, W. T., and Goodman, R. H. (2003) Differential binding of NAD^+ and NADH allows the transcriptional corepressor carboxyl-terminal binding protein to serve as a metabolic sensor, *Proc. Natl. Acad. Sci. U.S.A. 100*, 9202−9207.

BI700170M